Hindawi
International Transactions on Electrical Energy Systems
Volume 2023, Article ID 3118713, 13 pages
https://doi.org/10.1155/2023/3118713

Research Article

Analysis of the Application and Benefits of Aircraft Electric Wheel Systems during Taxi and Take-Off

Shuang Sun, Yu Liao, Shuo Ding, Yinte Lei, Song Li, Zhijie Hu, and Hualong Dong

Civil Aviation University of China, Tianjin 300300, China

Correspondence should be addressed to Yinte Lei; 2021012128@cauc.edu.cn

Received 15 September 2023; Revised 3 November 2023; Accepted 6 November 2023; Published 18 November 2023

Academic Editor: Sujin Bureerat

An electric wheel hybrid power system is designed for driving a large single-aisle passenger aircraft during the take-off and ground taxi phases, which consists of an APU, an energy storage system, and a motor. In the taxi phase, the electric wheel hybrid power system works alone, and the turbofan engine does not work, reducing fuel consumption and pollution emissions. During the take-off rolling phase, the electric wheel hybrid power system and turbofan engine work together to reduce the thrust requirement of the turbofan engine. This article establishes an aircraft kinematic model, hybrid power system model, and a mechanical wheel model. The feasibility of the collaborative work of the electric wheels and the turbofan engines is verified by simulations. By utilizing the established hybrid system of electric motor wheels, the fuel consumption can be reduced, and the emissions of CO, HC, and NO_X can also be diminished to varying degrees. The input of motor power leads to lower turbine inlet temperature, thereby enhancing the turbofan engine's service life by approximately 4.3% and saving operational costs.

1. Introduction

Civil aviation aircraft are usually launched from their berths using a tractor, and the aircraft starts the main engines and runs on the taxiway to the end of the runway for take-off [1–3]. During this process, the time required to tow the aircraft is long, the fuel economy of the main engine during the taxi phase is poor, and pollution emissions are high [4]. To reduce operating costs, pollution, and greenhouse gas emissions, the industry has proposed an electric wheel system to replace the main engine for driving aircraft to the end of the runway. Honeywell and Safran have jointly developed the EGTS (Electric Green Taxiing System) solution for civil aircraft [5]. The EGTS solution uses electric motors mounted on the main landing gear wheels to drive the aircraft and can reduce fuel consumption by nearly 4% per flight for an A320. That reduces 75% of carbon emissions and 50% of nitrogen oxide emissions during the taxi phase, which helps airlines save $20 k–45 k per year per airplane. Wheel Tug has developed a power wheel mounted on the front landing gear of an aircraft [6] to replace the main engine during the taxi phase. The advantage of this solution is that it does not interfere with the arrangement of the main wheel brake discs and that only the front wheel lateral deflection needs to be controlled during ground turns without differential control of the main wheel torque.

Huang et al. [7] noted theoretically that an electric wheel system can play a role in improving the heading direction load during the landing stage. Heinrich et al. [8] compared the energy consumption of four groups of aircraft equipped with electric wheel systems and showed that electric wheel systems are generally energy efficient for aircraft. Re and Castroy [9] assessed the best path for aircraft taxi with a specific electric driver system architecture. This study used the minimum fuel and taxi path as the optimization target. The APU (auxiliary power units) provides electrical energy for the electric taxi system and uses optimization methods to minimize fuel consumption. Recalde et al. [10] studied a battery-driven electric taxi system, reducing the fuel consumption in the aircraft taxi process through offline optimization and analyzing the life cycle of the battery. Dzikus and Schaefer [11] modeled fuel consumption for short-medium distance aircraft in three modes: electric taxiing, operational towing, and single-engine drive. Cheaito

et al. [12] assessed the feasibility of an aircraft electrical taxi system, analyzed the electrical characteristics, and designed a new energy storage system to solve the problem of insufficient APU power during the taxi phase.

To study the benefits of an electric wheel taxi system, based on the ICAO (International Civil Aviation Organization) database, Guo et al. [13] used the statistical software SAS to process the input data and studied the effects of differences in a complex environment and aircraft type on the fuel consumption and pollution emissions of aircraft on the ground at four airports under 10 operating conditions. The study showed that the energy saving and emission reduction benefits of the EGTS were much greater than those of other taxi methods. Barelli et al. [14] established a hybrid energy storage system consisting of $LiFePO_4$ batteries and supercapacitors. An emission performance evaluation model was developed to facilitate the performance study of the energy storage devices for electric taxi systems and the analysis of energy saving and emission reduction benefits. Hospodka [15] developed an economic model based on a study by Nikoleris et al. [16] and used an A320 aircraft with CFM56-5B engines as an example for calculation. The results showed that the electric taxi system saved 250 Euros per take-off and landing cycle, and each aircraft saved more than 250,000 Euros per year when using the electric taxi system, assuming an average of 1000 missions per year.

It should also be noted that engine maintenance costs account for approximately 40% of airline maintenance costs [17]. According to a report by SRI [18] and some estimations [19–21], the maintenance cost per hour of aircraft flight was approximately €750, of which engine maintenance costs were approximately €300 per hour. Reduction in turbofan engine take-off thrust reduces turbine entry temperatures and improves turbine hot end components, including the turbine creep life and low perimeter fatigue life. It reduced the frequency of removing the engine and, to some extent, reduced the number of spare airline engine, saving operating costs. Koudis et al. [22] conducted an analysis of the methods and the benefits of reduced thrust take-off, showing that reduced thrust take-off can delay engine performance degradation, extend their life, reduce maintenance costs and quantify the impact of reduced thrust on aircraft emissions. Zhang and Nie [23] studied the effect of thrust reduction on EGT (exhaust gas temperature) margins during take-off and showed a positive effect on engine performance degradation.

The aforementioned study primarily analyzes the feasibility and benefits of the taxiing phase. To tackle the high fuel consumption and pollution issues during the taxiing and rolling take-off phases, efforts are being made to find effective solutions. In order to maximize the benefits, this paper aims to increase the power of electric motor wheels, while simultaneously achieving electric taxiing during the taxi phase and wheel-assisted take-off during the rolling take-off. Taking the narrow-body aircraft B737–800 as the research platform, the feasibility of this concept is analyzed from the perspectives of aircraft kinematics and power systems. Therefore, suitable electric motors, transmission systems, and other components need to be selected to construct a hybrid system consisting of an auxiliary power unit (APU), an energy storage unit, and electric motors. Finally, the performance analysis of the aircraft equipped with the electric motor wheel hybrid system is conducted, and fuel savings are predicted using empirical theory. Based on the reduced engine thrust, the benefits of extending the engine life cycle in terms of wing hours were calculated.

2. Aircraft Take-Off Phase Performance Analysis

2.1. Aircraft Motion Model. In this paper, the B737–800 aircraft with tricycle landing gear arrangement was selected as the research platform for modeling and simulation analysis. The main parameters are shown in Table 1.

As shown in Figure 1, the flight mechanics are modeled using the airframe coordinate system. The origin point O is located at the mass center of the aircraft, and the axis O_{xb} is parallel to the fuselage axis segment or the mean aerodynamic chord of the wing, pointing in the direction of the nose. O_{yb} is along the direction of wing of the aircraft, and O_{zb} satisfies the right-hand rule. ψ, θ, and ϕ are the yaw, pitch and roll angles, respectively.

Based on the B737-8 design parameters, a six-degree-of-freedom model of the aircraft is established by converting the vector form to matrix form through rigid body mechanics. The force balance equation in the noninertial system is shown in equation (1). The equation of torque balance is represented by equation (2).

$$m\begin{bmatrix}\dot{U}\\ \dot{V}\\ \dot{W}\end{bmatrix} + m\begin{Vmatrix} ijk\\ PQR\\ UVW\end{Vmatrix} = \begin{bmatrix}F_x\\ F_y\\ F_z\end{bmatrix}, \tag{1}$$

$$\begin{bmatrix}\dot{P}\\ \dot{Q}\\ \dot{R}\end{bmatrix} = \mathbf{I}^{-1}\left(-\begin{bmatrix}P\\ Q\\ R\end{bmatrix}\times \mathbf{I}\begin{bmatrix}P\\ Q\\ R\end{bmatrix} + \begin{bmatrix}M_x\\ M_y\\ M_z\end{bmatrix}\right), \tag{2}$$

where m is the mass of the aircraft and the fuselage coordinate system. x, y, z are the three directions with a linear base of $[i, j, k]$ (which rotates around the ground coordinate system). P, Q, R are the angular rates of roll, pitch, and yaw of the airframe coordinate system around the ground coordinate system, respectively. U, V, W are the coordinate values of the velocity vector in the airframe coordinate system. F_x, F_y, F_z are the thrust forces in the three axis directions. $\mathbf{I}$ represents the product of inertia of the aircraft, and M_x, M_y, and M_z, respectively, denote the external torques acting on the x, y, and z axis of the body coordinate system.

2.2. Aircraft Take-Off Performance Analysis. Based on the six-degree-of-freedom mechanical model of aircraft motion, a simulation model was built using MATLAB/Simulink to proceed with the performance study. The simulation model built according to the study [24, 25] is shown in Figure 2. From equations (1) and (2), the dynamics, motion, and position equations can be derived together to form a six-degree-of-freedom attitude model. The simulation results

Table 1: Main parameters of the B737-8.

Parameters	Numerical values
Fuselage length (m)	39.5
Wingspan (m)	35.79
Overall height of aircraft (m)	12.5
Axial distance of main landing gear mounting point from the center of mass (m)	0.53
Lateral distance of main landing gear mounting point from the center of mass (m)	2.12
Mass (kg)	79250

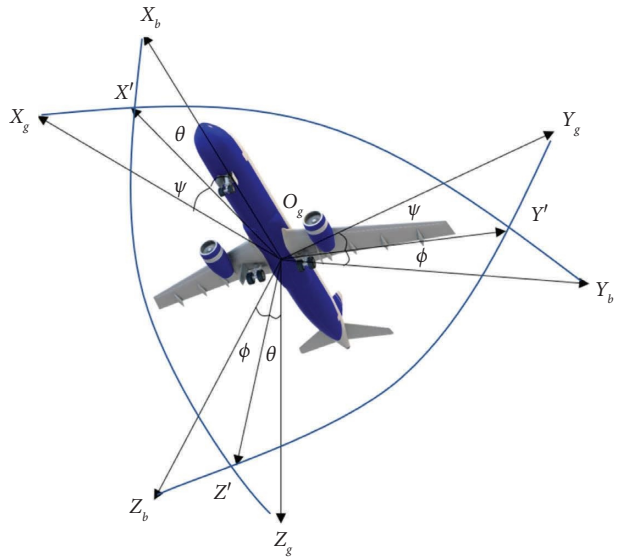

Figure 1: Coordinate system of the airframe.

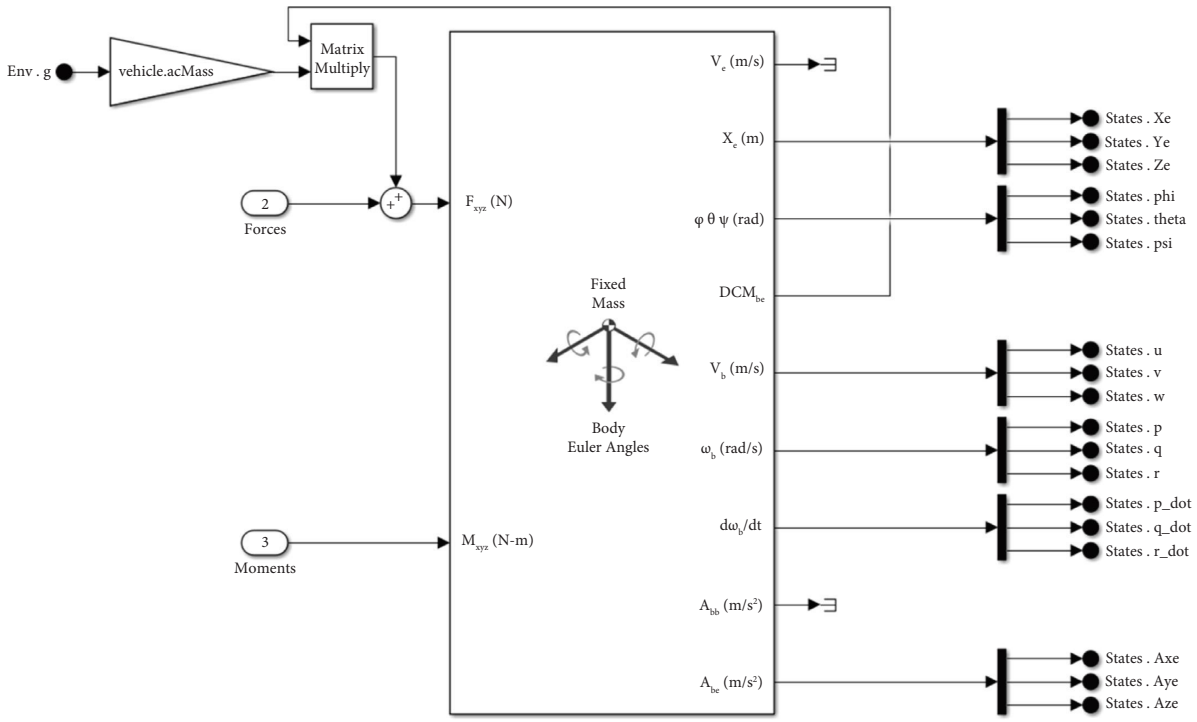

Figure 2: Six-degree-of-freedom model.

are obtained by converting between the geographic, airframe, and velocity coordinate systems, combined with 2D and multidimensional interpolation of the aerodynamic data. The main input and output variables of the simulation model are shown in Table 2.

The B737-8 is equipped with a CFM56-7B27 engine with a maximum thrust of 27300 lbf, which is approximately 121.354 kN, and a maximum speed of 15183 rpm. During take-off, the pilot adjusts the fuel supply by changing the position of the throttle lever, which is used as an input signal to change the engine speed and thrust [26]. Figure 3 shows the comparison between the simulation model and the experimental data during take-off. The experimental data are obtained from the QAR (quick access recorder) data of 737–800 aircraft with a sampling frequency of 1 Hz. At $t = 43$ s, the pilot was performing a front wheel lift at a ground speed of 140 kn ($v_{tr,T/O} = 140$ kn), so this speed point is selected as the end of the electric wheel operation in this study.

During the take-off rolling phase, the engine fuel flow rate is shown in Figure 3(a). This value rose gradually from 2700 kg/hr and was close to a peak value after 9 s. The fuel flow rate has small fluctuations during the remaining time of this phase. Figures 3(b) and 3(c) show the simulation results of the speed and acceleration of the corresponding process. The dashed line in Figure 3 represents the trend line fit by simulation or QAR data. As shown in Figure 3, the simulation results of the transients and trend line are in good agreement with the experimental values, so the simulation model can be used as a platform for subsequent analysis.

2.3. Engine Thrust Reduction Analysis. Electric motors and turbofan engines work at the same time during the take-off phase. The electric motor outputs power to achieve the reduction of turbofan engine thrust. The sum of the thrust of the turbofan engine and the thrust provided by the electric wheel is made to be the same as that of the original turbofan engine in real time. This ensures that the physical sensation of the passengers inside the aircraft is the same as that of the original aircraft.

According to the QAR data, the thrust and speed relationship of the turbofan engine can be obtained as shown in Figure 4(a). When the maximum engine speed is maintained at approximately 98% during take-off, the thrust of the engine is approximately 117.59 kN at this time. When the individual engine reduces 2% of the speed, the single-engine thrust is reduced by approximately 4.37 kN. When the individual engine reduces 1% of the speed, the single-engine thrust is reduced by approximately 2.06 kN.

Considering the actual performance of the electric motor, the thrust provided by the electric wheel in this study can reduce the speed of the turbofan engine by a maximum of 2%. In the QAR data, the aircraft takes off with the engine at 98% speed. With the use of a hybrid power system (HPS) consisting of an electric wheel and a turbofan engine, the engine plus motor power always matches the thrust of the original turbofan engine during take-off. As the aircraft ground speed continues to increase, the motor torque continues to decrease due to the performance limitations of the motor [27]. Therefore, the motor's boost to the aircraft during this process will begin to decrease. To adapt to the performance of the motor, the speed of the engine is reduced from 2% linearly to 1%. As shown in Figure 4(b), from 0 to 7 s, the turbofan engine accelerates from idling to a 96% speed state, and the motor does not work. From 7 to 43 s, the motor starts to intervene and gradually boosts the power output. At approximately 8 s, the overall thrust of the aircraft reaches the maximum value, and the thrust provided by the electric wheel also reaches a maximum of 8.74 kN. From 8 to 43 s, the thrust of the turbofan engine gradually increases, and the speed increases from 96% to 97%. The thrust provided by the electric wheel gradually decreases, maintaining the same take-off thrust of 235.2 kN.

2.4. Analysis of Aircraft Taxi Phase Thrust Requirements. The principle of motor-driven taxi of an aircraft is similar to that of a car. It needs to overcome rolling resistance, air resistance, acceleration resistance [28], etc. The maximum acceleration of the aircraft taxi phase is 0.25 m/s^2, at which point the required driving force $F_{tr,Taxi}$ is

$$F_{\text{tr,Taxi}} = G_f + \text{ma}, \tag{3}$$

where $F_{\text{tr,Taxi}}$ is the driving force required to generate the acceleration of the aircraft, m is the mass of the aircraft, a is the acceleration, and G_f is the rolling friction force. The relevant parameters for the aircraft and the electric-wheel system are given in Table 3. The result is $F_{\text{tr,Taxi}} = 27579$ N according to the relevant data of Table 3.

3. Hybrid Power System Analysis

3.1. Hybrid Power System Construction. The hybrid system constructed in this study consists of motors, transmissions, energy storage, and gas turbines, and four motors are located on the four wheels of the main landing gear. The APU and energy storage system provide power to the wheels and are controlled by the electronic power components. The motors are connected to the wheels via a reduction gearbox, which matches the torque and power between the motors and the wheels. To verify the performance of the powertrain, an energy management strategy for the hybrid powertrain is given in Figure 5, based on previous studies [29, 30]. The APU provides the electrical energy required during the approximately 10-minute taxi, with the energy storage system not operating, and this configuration was validated in the study [31]. During the take-off phase, the APU and the energy storage system are simultaneously at the maximum power output state during the approximately 43 s period. The power provided by energy flow 1 and 2 is transferred by the electronic assembly to the four electric motors, which in turn actuate the wheels of the aircraft's main landing gear through a planetary reduction gearbox.

Table 2: Main input and output variables of the simulation model.

Parameter symbol	Parameter category	Unit
Input		
F_{xyz}	Aircraft resultant force	N
M_{xyz}	Aircraft resultant moment	N · m
Output		
V_b	Aircraft line speed	m/s
A_{be}	Aircraft resultant acceleration	m/s^2
ω_b	Angular velocity of aircraft	rad/s
φ, θ, ψ	Euler angles	rad
X_e	Aircraft reference system position points	m
DCM_{be}	Position points after reference system conversion	m

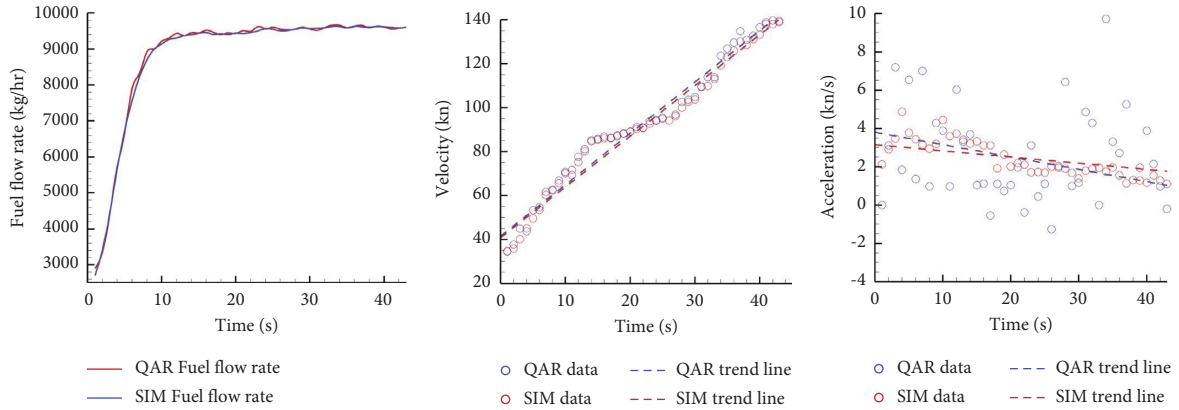

Figure 3: Comparison of simulation data with experimental data. (a) Fuel flow rate. (b) Speed-time. (c) Acceleration-time.

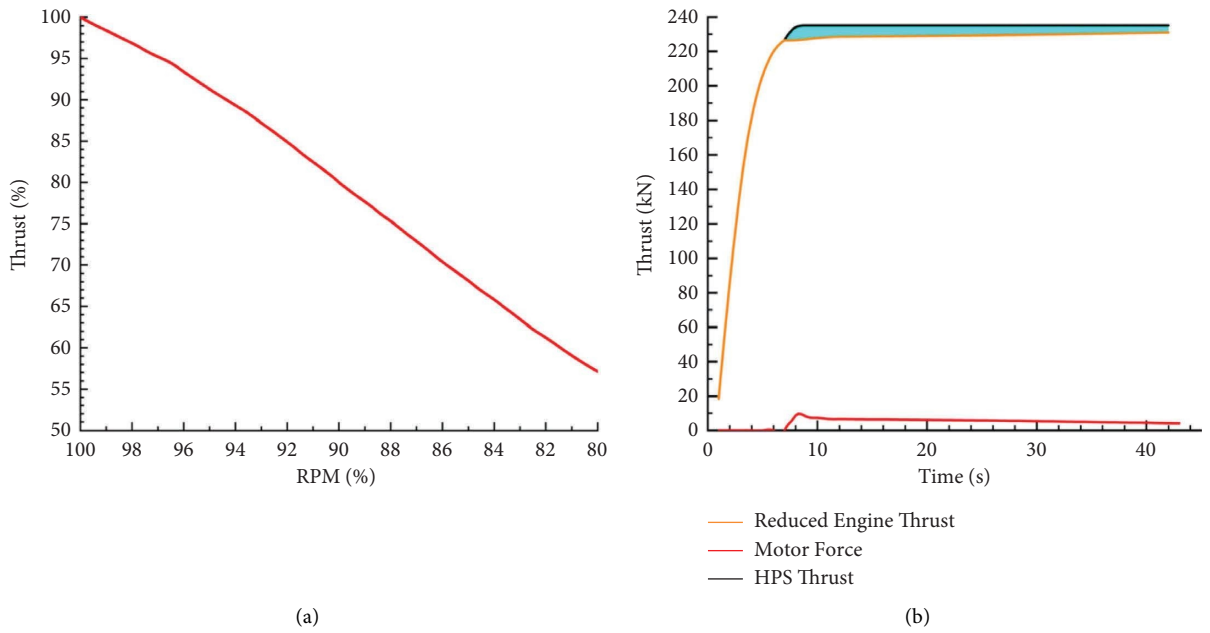

Figure 4: Thrust relationship under reduced thrust conditions. (a) Thrust-engine speed. (b) Thrust-time.

Table 3: Parameters of the electric wheel system.

Parameter category	Parameter symbols	Numerical values
Mechanical transmission efficiency	η_1	0.98
Motor work efficiency	η_2	0.91
Rolling friction coefficient	μ_1	0.01
Wheel radius	R_W	55 cm
Aircraft mass	m	79250 kg

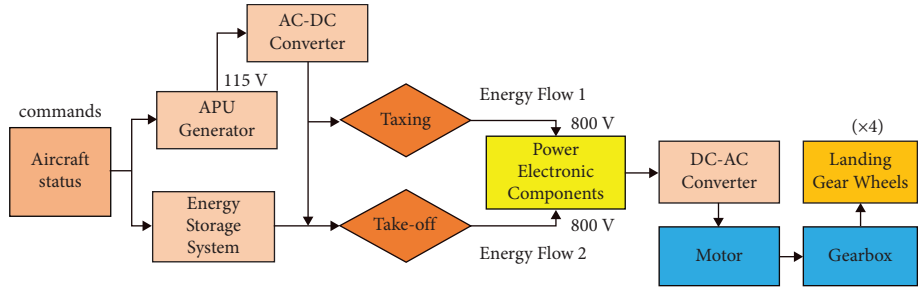

Figure 5: Energy flow diagram.

3.2. Selection of Permanent Magnet Synchronous Motors. The electric motor plays an auxiliary role in the taxi and take-off phases. The sum of the thrust provided by the turbofan engine after thrust reduction and the electric wheel is the same as the original engine in real time as shown in the following equation:

$$F_{\text{Engr}} + F_{\text{Motor}} \approx F_{\text{Eng}}, \tag{4}$$

where F_{Engr} is the thrust of the HPS turbofan engine after thrust reduction, F_{Motor} is the thrust to be provided by the electric wheel, and F_{Eng} is the thrust required by the original aircraft during the take-off phase. Four motors are arranged on the four wheels of the main landing gear, and each motor drives the wheel movement via a planetary reduction gearbox. The analysis of electric motor power and other performance metrics are conducted by both the taxi and rolling take-off phases.

3.2.1. Aircraft Taxi Phase. The electric motor and the single wheel of the main landing gear need to provide torque.

$$T_2 = 0.25 R_W \cdot F_{\text{tr,Taxi}}, \tag{5}$$

$$T_1 = \frac{T_2}{i * \eta_1}, \tag{6}$$

where T_2 is the torque required to be generated by a single wheel, T_1 is the torque required produced by a single motor, the gear ratio i is chosen as 10, R_W is the radius of the machine wheel, and η_1 is the gearing efficiency. According to equation (3), the driving force $F_{\text{tr,Taxi}} = 27579$ N. Furthermore, the electric wheel system needs to be matched to the aircraft's ground speed. The motor and wheel speeds during the taxi phase are calculated by the following equations:

$$n_1 = i \cdot n_2, \tag{7}$$

$$n_2 = \frac{v_{\text{tr,Taxi}}}{2\pi R_W}, \tag{8}$$

where n_1 is the maximum speed of the motors, n_2 is the maximum speed of the wheels, and $v_{\text{tr,Taxi}}$ is the maximum ground speed during the taxi phase of 10 m/s.

3.2.2. Aircraft Rolling Take-Off Phase. The analysis methodology for the take-off phase is consistent with that of the taxi phase, although the required propulsion force provided by the motor differs. During the aircraft's rolling take-off phase, the maximum propulsive force offered by all motors is equal to thrust lost due to a 2% decrease in engine speed. At this moment, the driving force $F_{\text{tr},T/O} = 8.74$ kN. By substituting the value into equations (5) and (6), we can determine the maximum torque requirement of motor during the rolling take-off phase. The electric wheel system needs to match the aircraft's max ground speed in the rolling take-off phase. The max ground speed $v_{\text{tr},T/O} = 72.02$ m/s. By substituting the value into equations (7) and (8), we can determine the maximum speed requirement of motor during the rolling take-off phase.

Combined with the analysis of rolling take-off phase and taxi phase, the maximum motor operating parameters can be determined as $T_{\text{motor, max}}$ and $n_{\text{motor, max}}$, which need to satisfy the following equations:

$$\begin{aligned} T_{\text{motor,max}} &= \max[T_1, T_1{}'] \\ &= \max[387, 122.5] \\ &= 387N \cdot m, \end{aligned} \tag{9}$$

$$\begin{aligned} n_{\text{motor,max}} &= \max[n_1, n_1{}'] \\ &= \max[1736, 12504] \\ &= 12504\text{rpm}, \end{aligned} \tag{10}$$

where T_1' is the torque required produced by a single motor in the rolling take-off phase. n_1' is the maximum speed of the motors in the rolling take-off phase. According to the plan of the thrust output and speed of the electric wheel in the take-

off phase, the plan of the total output power demand of the wheel can be obtained as shown in Figure 6. At $t = 37$ s, the maximum machine wheel output power is 317.6 kW, and the total peak motor power after considering the component efficiency needs to be $P_t = 356.1$ kW.

The motor needs to meet maximum torque requirements, speed requirements, and power demand. Therefore, the performance diagram for the selected individual PMSM (Permanent Magnet Synchronous Motor) is shown in Figure 7. The main performance indicators are shown in Table 4. The motor was initially designed and calibrated by Tianjin Santroll Electrical Technology, Co., Ltd.

3.3. Selection of the Drive System. The electric wheel system requires a large torque output from the main wheel at high operating speeds, so a reduction gearbox needs to be added between the main wheel and the motor to increase the torque of the main wheel. To achieve the requirement of a gear ratio $i = 10$ while considering space and transmission efficiency, the planetary wheel system is selected as the reduction gearbox, whose configuration satisfies the following conditions:

$$\begin{aligned} r_H &= r_s + r_p, \\ r_H\omega_H &= r_s\omega_s + r_p\omega_p, \\ r_g &= r_H + r_p, \\ r_g\omega_g &= r_H\omega_H + r_p\omega_p, \end{aligned} \tag{11}$$

where r_H is the radius of the planetary frame, ω_H is the angular velocity of the planetary frame, r_s is the radius of the sun wheel, ω_s is the angular velocity of the sun wheel, r_p is the radius of the planetary wheel, ω_p is the angular velocity of the planetary wheel, r_g is the radius of the gear ring, and ω_g is the angular velocity of the gear ring. A sketch of the structure of the reduction gearbox is shown in Figure 8.

Due to the limited space between the main landing gear wheels of the B737-8, the center distance between the sun wheel and the planetary wheel of the gearbox was determined by referring to the existing main landing gear wheel spacing, which has a center distance of 80 mm and a gear module of $m = 2.5$. The relevant parameters were obtained according to the relevant design manual [32] and research data as shown in Table 5.

3.4. Design and Selection of Energy Storage System. According to the electric wheel system designed in this paper, the motor only provides auxiliary power during the take-off and taxi phases. Therefore, energy storage only needs to meet the consumption of the take-off and taxi phases. In response to this high-level discharge rate demand, supercapacitors are usually selected. Supercapacitors have better power characteristics than lithium batteries, and their charge and discharge rates are relatively high, but the drawback is that their power density is low.

Because supercapacitors have a high output power, matching parameters do not take into account the power effect in the early stage. This is calculated from the following equations:

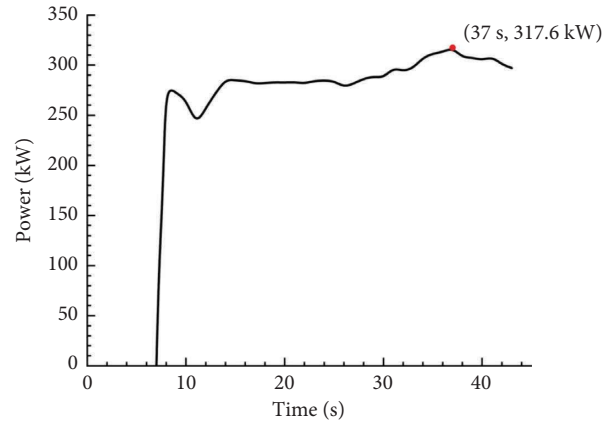

Figure 6: Power demanded by the machine wheel.

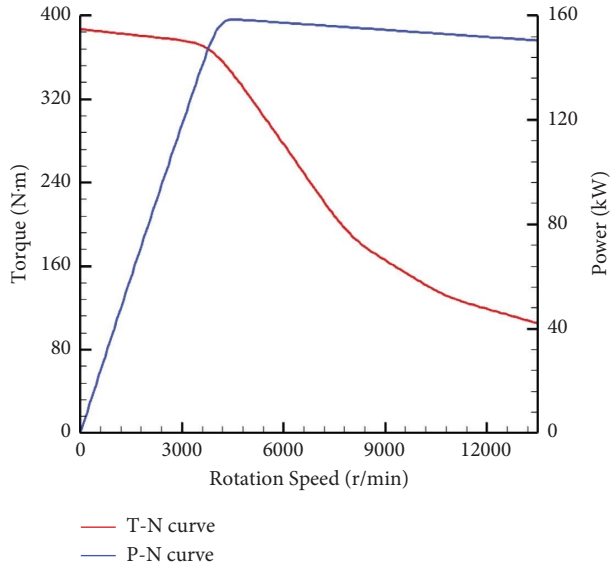

Figure 7: Motor performance parameters.

Table 4: Basic parameters of permanent magnet motors.

Motor parameters	Numerical values
Maximum speed	13500 rpm
Maximum torque	390 N · m
Maximum power	159 kW
Total mass	70 kg
Diameter	380 mm
Axial length	130 mm
Operating voltage	320 V

$$\begin{aligned} E_{\mathrm{sc}} &= \frac{1}{2} \cdot C_{sc} \cdot \left(U_{sc}^2 - U_{sccf}^2\right), \\ U_{sc} &\leqslant 800V, \\ U_{sccf} &\geqslant 500V, \end{aligned} \tag{12}$$

where U_{sc} is the maximum operating voltage of the supercapacitors, U_{sccf} is the cutoff voltage, E_{sc} is the available energy, and C_{sc} is the capacitance of the supercapacitor. The

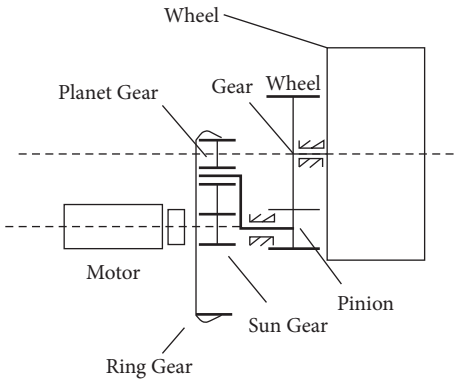

Figure 8: Gearbox scheme.

Table 5: Gearbox parameters.

Parameter category	Specific values
Number of teeth on the ring z_1	56
Number of large gear teeth z_2	68
Number of small gear teeth z_3	28
Number of teeth on the planetary wheel z_4	18
Number of sun wheel teeth z_5	20
Ring diameter d_1	140 mm
Large gear diameter d_2	170 mm
Small gear diameter d_3	70 mm
Center distance	77.5 mm

calculation shows that $C_{sc} \geq 97$F. If all the supercapacitors are connected in series, the number of supercapacitors is approximately 296, which means that the capacitance of a single supercapacitor is at least 28712 F. If the individual capacitance is less than 28712 F, the capacitance can be increased by a parallel connection. The capacitance of the 2.7 V/29000 F graphene nanohybrid super Faraday capacitor can meet the demand with a single mass of 0.55 kg, and the total mass is 163 kg.

The matching results of the main parameters of the supercapacitor are shown in Table 6, which basically meet the index requirements.

3.5. Hybrid Power System Performance Summary. The loading of a hybrid power system leads to an increase in the total weight of the aircraft, which may affect the additional consumption of aircraft fuel. Weight is a key driver in the assessment of the feasibility of hybrid power systems. Based on the analysis of the above components and the determination of various component specifications in hybrid power systems, combined with the assessment of the electric taxi system in the literature [33], the main general parameters of the hybrid system are given in Table 7. Due to a large number of new electrical components, the temperature of the electrical components must be maintained at their respective appropriate operating temperature during system operation. Therefore, a cooling system for the electrical components is required to allow the electric propulsion system to operate properly. The mass evaluation of the cooling system refers to the specifications of liquid/air radiators in the literature [34, 35].

Table 6: Supercapacitor parameter specifications.

Parameters	Numerical value
Number of series and parallel connections	296 S
Max working voltage	794 V
Minimum working voltage	500 V
Nominal capacity	97 F
Mass	163 kg
Available energy	7186 wh

Table 7: General parameters of the hybrid power system.

Parameters	Numerical value
Maximum system power	487.1 kW
Maximum motor power	356.1 kW
Maximum bus operating voltage	≈800 V
Maximum system heat output	131 kW
Total system mass	677 kg
Cooling system mass	60 kg
Total motor mass	280 kg
Total inverter mass	14 kg
Total rectifier mass	6 kg
Supercapacitor mass	163 kg
Cable mass	104 kg
Other	50 kg

4. Analysis of Simulation Results

4.1. Analysis of the Take-Off Performance of the Electric Wheel Hybrid Power System. Aircraft equipped with an electric wheel system can use the driving control method of electric vehicles. The simulation program is established as shown in Figure 9 below. In the aircraft ground motion model, considering the environment, state, and other comprehensive factors, by providing input signals to the system, the aerodynamic module outputs the aerodynamic force and moment of the aircraft at this time. The pilot can control the position of the throttle according to the aircraft's status to control the thrust output of the engine. The energy storage system transfers the energy to the electric motor, and the electric motors transfer the energy to the aircraft wheel. The total sum force and total moment of the aircraft are input to the six-degree-of-freedom module. This paper uses the motion and position equations together to form a six-degree-of-freedom attitude model. It can match the thrust required for the aircraft and input the required sum force and sum moment to obtain the speed and acceleration of the aircraft. The disturbance load of the motors is consistent when the aircraft is running in a straight line. The operation process is in the ideal synchronous state, and the aircraft in this state is simulated by combining the environment model and the dynamics model.

Figure 10 shows a comparison of the take-off simulation results between the HPS and turbofan engine conditions. The condition in which only the engine works during the take-off phase of the aircraft without a hybrid power system is called turbofan engine in the following article, and the condition with the electric wheel hybrid power system is called HPS below. In Figure 10(a), the aircraft speed gradually increases during the 43 s simulation time, and the

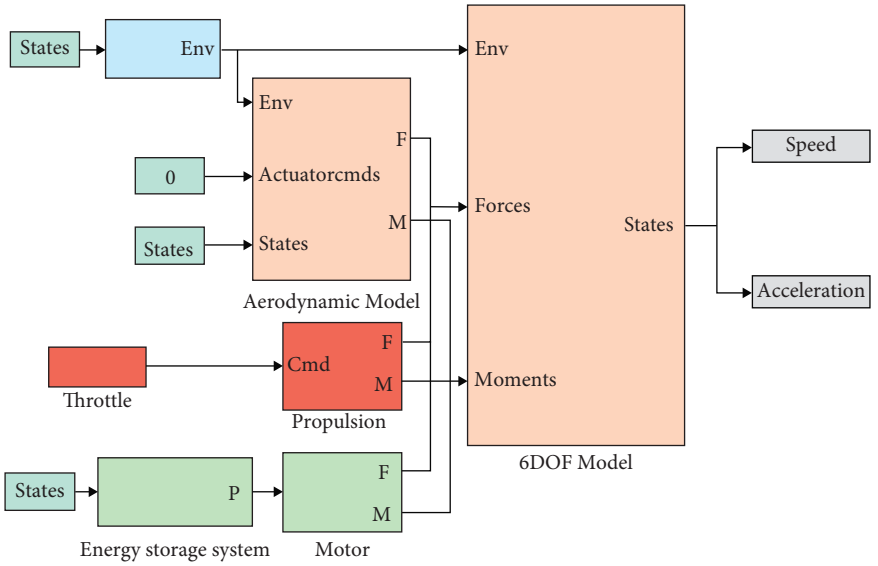

Figure 9: Simulation model of an aircraft with a hybrid powertrain.

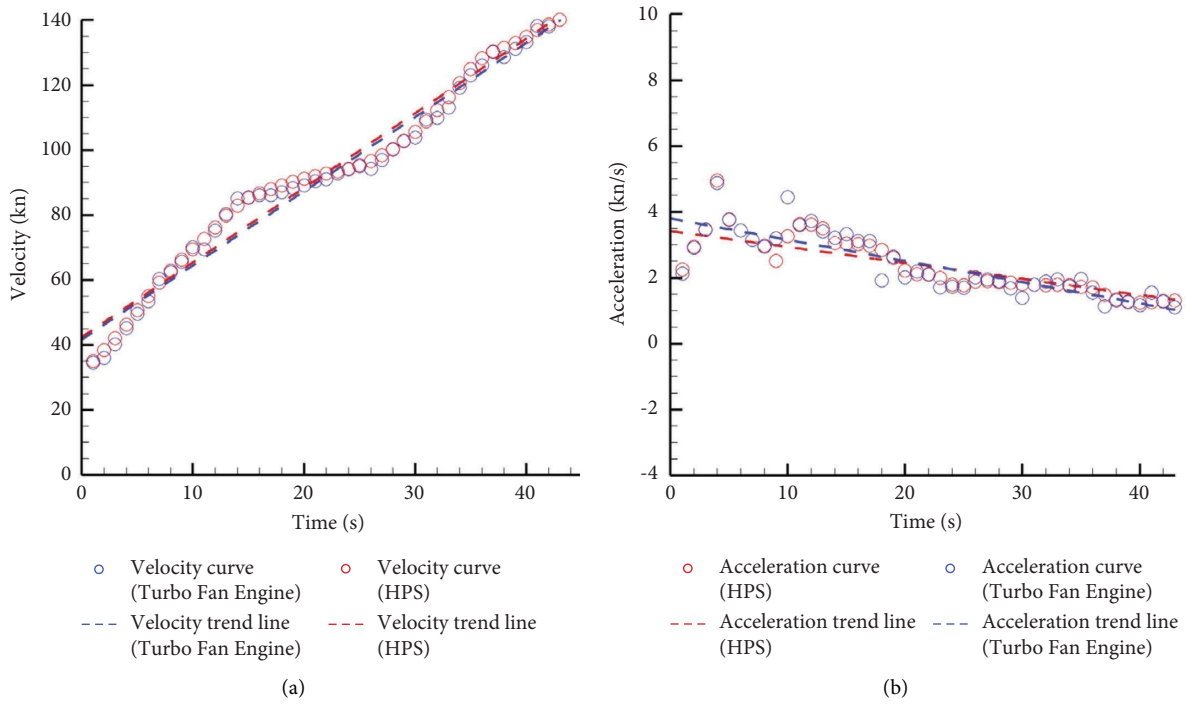

Figure 10: Comparison of velocity and acceleration under the two conditions. (a) Velocity-time. (b) Acceleration-time.

HPS and turbofan Engine reach a lifted front wheel speed of $v_{tr,T/O} = 140$ knots at 43 s. Since the motors in the HPS and the engine are deviation-coupled controls with good synchronization, the speed trend lines of the HPS and the turbofan Engine are almost identical under the same simulation conditions, indicating that the HPS design in this paper meets the speed requirements of the aircraft with a reduced speed and thrust engine. As shown in Figure 10(b), the acceleration of the HPS and turbofan Engine does not fluctuate significantly during the 0–7 s period because the motor does not intervene, and only a small weight deviation occurs. From 7 to 43 s, the HPS design power meets the demand power, and the driving performance is almost consistent with the turbofan engine. For the two driving methods, the maximum acceleration of the HPS can reach 4.95 kn/s, and its minimum acceleration is 1.31 kn/s. The turbofan engine has a maximum acceleration of 4.93 kn/s and a minimum acceleration of 1.10 kn/s. Compared with the trend line in Figure 10(b), the HPS acceleration is gentler, and the passengers will be more comfortable.

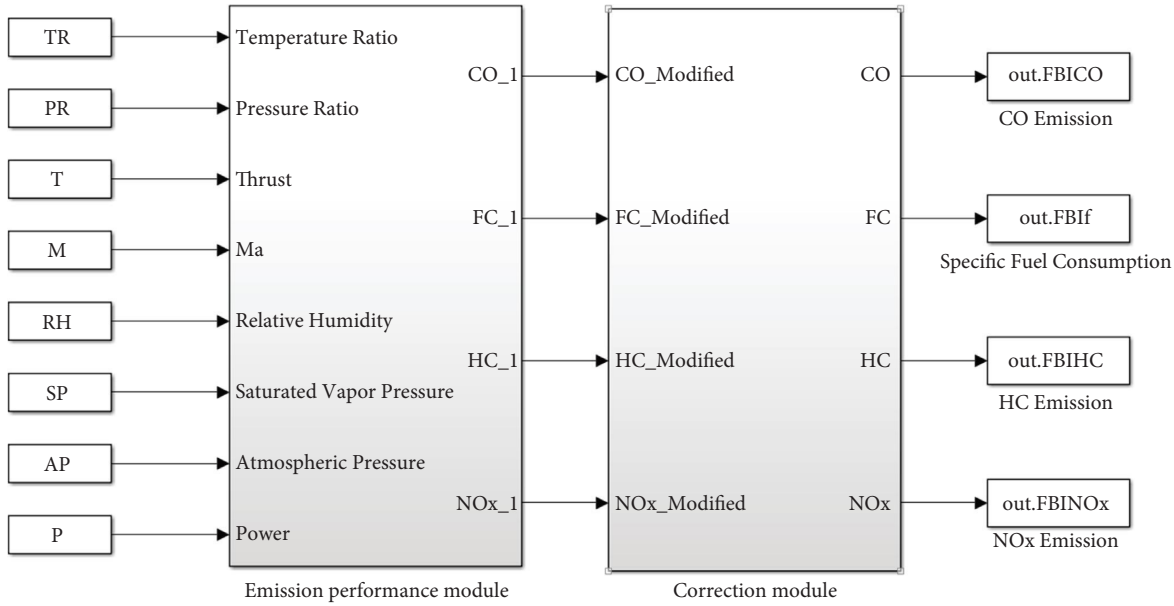

Figure 11: Calculation model for fuel consumption and emissions.

4.2. Emission Benefits Prediction. This paper compares the emissions of a B737-8 aircraft equipped with the original turbofan engine and the same aircraft equipped with the HPS (which brings 677 kg extra mass) using Beijing Capital International Airport (ZBAA) as the take-off airport and Shanghai Hongqiao Airport (ZSSS) as the landing airport, with a total flight time of two hours. The preset taxi period from the corridor to the starting point of take-off is approximately 10 minutes. The take-off rolling time is 43 s. Based on the performance parameters of the CFM56-7B27 engine and the GTCP36–300 APU and QAR data, a simulation model of fuel consumption and emissions is established as shown in Figure 11.

The emission performance model in Figure 11 consists of five different modules for the taxi, take-off rolling, climb, cruise, and approach phases. By inputting the appropriate environmental and airframe performance parameters and calculating the fuel consumption rate in the function module, rough pollutant emissions and fuel consumption can be obtained for each phase of the aircraft in both drive modes [36]. However, only CO_2 is proportional to fuel consumption among all pollution sources, and the other emissions need to be corrected by a factor. For this reason, the emission model of the entire flight stage needs to be corrected. The correction process needs to convert the fuel flow of the aircraft into a correction fuel flow under ISA (International Standard Atmosphere) conditions, so the correction module was established after the emission performance module. This module is based on the ICAO's baseline fuel flow rate and the corresponding pollutant emission index [37]. First, it establishes a fitting formula to obtain the corrected emission rate function for each pollutant and fuel consumption, and then it obtains the fuel consumption and each pollutant emission by integration. Each correction factor is shown in Table 8.

Using the fuel consumption and emissions simulation model shown in Figure 11, the fuel consumption and associated gas emissions are simulated for both drive modes. Table 9 shows the results of the comparison of fuel consumption and associated emissions for the two different drive modes. Adding up the emissions of each stage for different driving modes separately, we can obtain a reduction of 2131.6 g of total CO, 220.3 g of total HC, and 92.3 g of total NOx in the HPS mode. In Table 9, the original aircraft configuration is 677 kg lighter than the HPS due to the absence of the electric wheel system, but the fuel consumption is 6158.04 kg, and the HPS case still saves 76.05 kg of fuel. The benefit is mainly due to the power output of the motor of the taxi and the take-off phase. However, the extra weight brought by the HPS during the flight phase increases the emissions and fuel consumption. In combination, the use of HPS has considerable benefits in terms of green development in the civil aviation industry.

4.3. Engine In-Wing Life Benefit Analysis. Engineering generally determines the engine removal time through the EGT margin. This method first assesses the EGT margin and predicts the remaining life by the EGT decay rate and the number of cycles installed, calculated as follows:

$$\mathrm{Cycle}_{\mathrm{Re}} = \left(\frac{\mathrm{EGTM}_C}{\mathrm{EGTD}_{\mathrm{ecay}}}\right) * 1000. \tag{13}$$

In the above equation, $EGTM_C$ denotes the engine exhaust temperature margin, $\mathrm{EGTD}_{\mathrm{ecay}}$ denotes the engine exhaust temperature decay rate, and $\mathrm{Cycle}_{\mathrm{Re}}$ denotes the number of cycles remaining. Based on the remaining life obtained, the removal time of the engine can be determined. Studies by Yin and Li [38] and Zhao et al. [39] indicate that there is a relationship between the segment ratio (the time

Table 8: Fuel consumption and correction factors for each emission.

Fuel consumption and emission categories	Correction factor
Fuel consumption flow rate	$\beta^{3.80}/\delta \cdot \mathrm{E}(0.2Ma^2)$
CO emission rate	$\beta^{3.30}/\delta^{1.02}$
HC emission rate	$\beta^{3.30}/\delta^{1.02}$
NOx emission rate	$\beta^{3.30}/\delta^{1.02} \cdot \mathrm{E}(19(0.0063 - 0.0062\varphi \cdot P_V/P_a - \varphi \cdot P_V))$

Table 9: Fuel consumption and associated gas emissions by phase.

Phase	Mode	Fuel (kg)	CO (g)	HC (g)	NOx (g)
Taxi	HPS	14.3	292.9	11.4	209.9
	Turbofan engine	139.2	2491.7	236.6	668.2
Take-off	HPS	96.6	19.3	9.7	2985.7
	Turbofan engine	110.4	22.1	11.0	3412.1
Climb	HPS	2276.7	1138.4	227.7	53957.9
	Turbofan engine	2252.9	1126.4	225.3	53393.3
Cruise	HPS	1874.4	2980.0	187.4	39737.5
	Turbofan engine	1854.7	2948.7	185.5	39320.1
Approach	HPS	1820.0	2547.9	182.0	20019.6
	Turbofan engine	1800.8	2521.2	180.1	19809.2
Total	HPS	6082.0	6979.2	618.2	116910.6
	Turbofan engine	6158.0	9110.1	838.5	117002.9

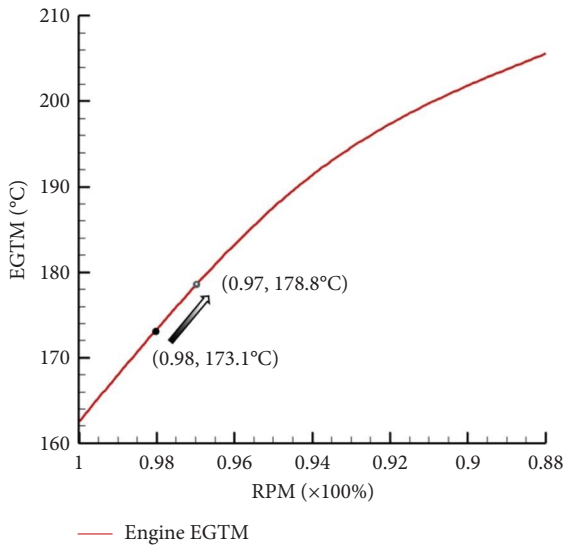

Figure 12: EGT margins.

used for a cycle) and the EGT decay rate provided to the airline by the civil aviation engine manufacturer. Therefore, the EGT decay rate of the engine can be determined by the hourly segment ratio of the aircraft. Using the relationship of the engine segment ratio and EGT decay rate [40], the EGT decay rate is 6.6°C/1000 hours based on a segment ratio of 2 for the B737-8 aircraft flight path studied in this paper, which is equivalent to 13.2°C/1000 cycles for the flight path studied in this paper. This paper shows the relationship between the engine speed change and the EGTM of the engine. As shown in Figure 12, when the engine speed is reduced from 98% to 97%, the EGT margin increases by 5.7°C compared to normal take-off. Assuming 10000 on-wing cycles for the original CFM56 brand new engine, according to the above description, the engine with the hybrid power system has 10431 on-wing cycles, and the HPS extends the engine life by 4.3%.

5. Conclusion

In this paper, a B737–800 loaded with an electric wheel system is studied, and its performance prediction and benefit analysis during the take-off phase are carried out. Based on an HPS design with a maximum power of 487.1 kW, a total system weight of 677 kg, and a maximum bus operating voltage of approximately 800 V, a simulation model of the aircraft with the electric wheel system was developed on the MATLAB/Simulink simulation platform. There is no significant change in the trend of speed variation for the two driving modes, and the maximum ground speed is reached almost simultaneously. Due to the intervention of the motor, the trend of HPS acceleration changes is relatively gentle. The simulation results show that the designed HPS has good stability and that the system meets the actual engineering requirements. It is feasible in the field of civil aviation.

The fuel consumption and pollutant emissions, as well as the EGT life prediction of this system, show that there are different degrees of energy saving and emission reduction effects in the taxi and take-off phases. For a two-hour flight segment, approximately 76 kg of fuel was saved per flight, while CO was reduced by approximately 2131.6 g, HC by approximately 220.3 g, and NOx by approximately 96.3 g. The engine life of an aircraft equipped with this system can be extended by approximately 4.3%. The HPS designed in this paper can effectively reduce energy consumption and pollutant emissions and increase the life of the turbofan engine, which improves the airline's operating economy in various aspects.

Data Availability

The data used to support the findings of this study are available from the corresponding author upon request.

Conflicts of Interest

The authors declare that there are no conflicts of interest regarding the publication of this paper.

Acknowledgments

This paper was supported by the Science Center for Gas Turbine Project (2022-B-II-008).

References

[1] R. González and E. B. Hosoda, "Environmental impact of aircraft emissions and aviation fuel tax in Japan," *Journal of Air Transport Management*, vol. 57, pp. 234–240, 2016.

[2] S. M. L. Soepnel, "Impact of electric taxi systems on airport apron operations and gate congestion at AAS," *AIAA Journal*, vol. 42, 2015.

[3] P. J. Ansell and K. S. Haran, "Electrified airplanes: a path to zero-emission air travel," *IEEE Electrification Magazine*, vol. 8, no. 2, pp. 18–26, 2020.

[4] B. J. Brelje and J. R. R. A. Martins, "Electric, hybrid, and turboelectric fixed-wing aircraft: a review of concepts, models, and design approaches," *Progress in Aerospace Sciences*, vol. 104, pp. 1–19, 2019.

[5] P. C. Roling, P. Sillekens, R. Curran, and W. D. Wilder, "The effects of Electric Taxi Systems on airport surface congestion," in *Proceedings of the 15th AIAA Aviation Technology, Integration, and Operations Conference*, Dallas, TX, USA, June 2015.

[6] M. Gubisch, "WheelTug is not for turning: manufacturer of nose-gear electric Taxi system remains confident in its product despite lack of support from airframers," *Flight International*, vol. 233, no. 6, 2014.

[7] M. Huang, H. Nie, and M. Zhang, "Analysis of ground handling characteristic of aircraft with electric taxi system," *Proceedings of the Institution of Mechanical Engineers- Part D: Journal of Automobile Engineering*, vol. 233, no. 6, pp. 1546–1561, 2018.

[8] M. Heinrich, F. Kelch, P. Magne, and A. Emadi, "Regenerative braking capability analysis of an electric taxiing system for a single aisle midsize aircraft," *IEEE Transactions on Transportation Electrification*, vol. 1, no. 3, pp. 298–307, 2015.

[9] F. Re and R. D. Castroy, "Energetically optimal path following for electric aircraft Taxi systems based on convex optimization," in *Proceedings of the 2014 IEEE International Electric Vehicle Conference (IEVC)*, pp. 17–19, Florence, Italy, December 2014.

[10] A. Recalde, M. Lukic, A. Hebala et al., "Energy storage system selection for optimal fuel consumption of aircraft hybrid electric taxiing systems," *IEEE Transactions on Transportation Electrification*, vol. 7, no. 3, pp. 1870–1887, 2021.

[11] N. Dzikus and M. Schaefer, "A forecast model to determine the potential for fuel savings through electric taxiing at airports," *Journal Proceedings of International Workshop on Aircraft System Technologies*, vol. 12, 2013.

[12] H. Cheaito, B. Allard, and G. Clerc, "Proof of concept of 35 kW electrical taxiing system in more electrical aircraft for energy saving," *International Journal of Electrical Power & Energy Systems*, vol. 130, Article ID 106882, 2021.

[13] R. Guo, Y. Zhang, and Q. Wang, "Comparison of emerging ground propulsion systems for electrified aircraft Taxi operations," *Transportation Research Part C: Emerging Technologies*, vol. 44, pp. 98–109, 2014.

[14] L. Barelli, G. Bidini, P. A. Ottaviano, F. Gallorini, and D. Pelosi, "Coupling hybrid energy storage system to regenerative actuators in a more electric aircraft: dynamic performance analysis and CO2 emissions assessment concerning the Italian regional aviation scenario," *Journal of Energy Storage*, vol. 45, Article ID 103776, 2022.

[15] J. Hospodka, "Cost-benefit analysis of electric Taxi systems for aircraft," *Journal of Air Transport Management*, vol. 39, pp. 81–88, 2014.

[16] T. Nikoleris, G. Gupta, and M. Kistler, "Detailed estimation of fuel consumption and emissions during aircraft taxi operations at Dallas/Fort Worth International Airport," *Transportation Research Part D: Transport and Environment*, vol. 16, no. 4, pp. 302–308, 2011.

[17] B. Tarhan, O. Yetik, and T. H. Karakoc, "Hybrid battery management system design for electric aircraft," *Energy*, vol. 234, no. 2, Article ID 121227, 2021.

[18] L. McCreary, *The Economic Cost of FOD to Airlines*, Insight SRI Ltd, Hyderabad, India, 2008.

[19] A. Commerce, "A320 family maintenance analysis & budget," 2022, https://aviaforum.ams3.cdn.digitaloceanspaces.com/data/attachment-files/2009/03/381333_008dc1e0905d1e21a67d382389fa8679.pdf.

[20] J. Gu, G. Zhang, and K. W. Li, "Efficient aircraft spare parts inventory management under demand uncertainty," *Journal of Air Transport Management*, vol. 42, pp. 101–109, 2015.

[21] E. Cost, "Standard inputs for eurocontrol cost benefit analyses," 2013, https://citeseerx.ist.psu.edu/document?repid=rep1&type=pdf&doi=d66f28abf0c379e199b0a102a82ee0e175a4c933.

[22] G. S. Koudis, S. J. Hu, A. Majumdar, R. Jones, and M. E. Stettler, "Airport emissions reductions from reduced thrust takeoff operations," *Transportation Research Part D: Transport and Environment*, vol. 52, pp. 15–28, 2017.

[23] T. C. Zhang and Z. Nie, "Preliminary analysis of impact of reduced thrust takeoff on engine removal," *D-Journal Series*, vol. 20, 2017.

[24] B. L. Stevens, F. L. Lewis, and E. N. Johnson, *Aircraft Control and Simulation: Dynamics, Controls Design, and Autonomous Systems*, John Wiley & Sons, Hoboken, NY, USA, 2015.

[25] H. P. Zipfel, *Modeling and Simulation of Aerospace Vehicle Dynamics*, J. AIAA Education Series, Reston, VA, USA, 2nd edition, 2014.

[26] O. Zaporozhets, V. Isaienko, and K. Synylo, "Trends on current and forecasted aircraft hybrid electric architectures and their impact on environment," *Energy*, vol. 211, Article ID 118814, 2020.

[27] S. Ma, S. Wang, C. Zhang, and S. Zhang, "A method to improve the efficiency of an electric aircraft propulsion system," *Energy*, vol. 140, pp. 436–443, 2017.

[28] Z. Yu, *Automobile Theory*, China Machine Press, Beijing, China, 3rd edition, 2000.

[29] O. Walter, A. Tremel, M. Prenzel, S. Becker, and J. Schaefer, "Techno-economic analysis of hybrid energy storage concepts via flowsheet simulations, cost modeling and energy system design," *Energy Conversion and Management*, vol. 218, Article ID 112955, 2020.

[30] P. Hoenicke, D. Ghosh, A. Muhandes et al., "Power management control and delivery module for a hybrid electric

aircraft using fuel cell and battery," *Energy Conversion and Management*, vol. 244, Article ID 114445, 2021.

[31] S. R. Hashemi, A. M. Mahajan, and S. Farhad, "Online estimation of battery model parameters and state of health in electric and hybrid aircraft application," *Energy*, vol. 229, no. 1, Article ID 120699, 2021.

[32] R. Liu, *Guide for Strength Design of Aircraft landing Gear*, Sichuan Science and Technology Press, Sichuan, China, 1989.

[33] F. Re, "Model-based optimization, control and assessment of electric aircraft taxi systems," *D-J Series*, vol. 25, 2017, https://tuprints.ulb.tu-darmstadt.de/id/eprint/6239.

[34] T. Raminosoa, T. Hamiti, M. Galea, and C. Gerada, "Feasibility and electromagnetic design of direct drive wheel actuator for green taxiing," in *Proceedings of the 2011 IEEE Energy Conversion Congress and Exposition*, Phoenix, AZ, USA, September 2011.

[35] N. Heersema and R. Jansen, "Thermal management system trade study for SUSAN electrofan aircraft," *AIAA SCITECH 2022 Forum*, vol. 30, 2022.

[36] N. Li and H. F. Zhang, "Calculating aircraft pollutant emissions during taxiing at the airport," *Journal Acta Scientiae Circumstantiae*, vol. 37, no. 5, pp. 1872–1876, 2017.

[37] J. J. Tang and D. X. Guo, "Driving characteristics and energy saving and emission reduction performance of aircraft electric taxiing system," *Journal of Beijing University of Aeronautics and Astronautics*, vol. 58, 2020.

[38] H. Yin and Y. Li, "Reduced thrust take-off control law design for large commercial aircraft," in *Proceedings of the 6th International Conference on Mechatronics, Materials, Biotechnology and Environment*, pp. 404–409, Yinchuan, China, August 2016.

[39] Y. Zhao, M. Chen, and D. Li, "Design of reduced thrust for civil aircraft takeoff based on performance simulation," in *Proceedings of the Fifth International Conference on Traffic Engineering and Transportation System (ICTETS 2021)*, pp. 1089–1099, Chongqing, China, September 2021.

[40] Boeing Company, "Boeing b737-600/700/800/900 aircraft maintenance manual," 2010, http://wtruib.ru/boeing_737/amm/.